Multi-agent Robotic System (MARS) for UAV-UGV Path Planning and Automatic Sensory Data Collection in Cluttered Environments

ABSTRACT: There has been growing interest in increasing the application of robotic and automation technologies for building indoor inspection. However, the previous research on indoor robotic applications was limited to a single type of unmanned aerial/ground vehicle (UAV/UGV), each of which has certain limitations and constraints. Besides, the robotic systems suffer from inefficient control within cluttered indoor environments containing many obstacles. This paper presents a multi-agent robotic system (MARS) for automatic UAV-UGV path planning and indoor navigation to automate sensory data collection. The proposed MARS consists of a new system architecture that defines the attributes and data requirements for UAV and UGV indoor path planning. To improve indoor navigation in cluttered environments, an enhanced shunting short-term memory model is established to optimize the trajectory of UAV/UGV for data collection. Assessment of indoor navigation is conducted with a simulation-based approach and LiDAR SLAM. A mediating agent, which harnesses a control algorithm and information exchange mechanism, is proposed to interoperate UAV and UGV for automated data collection. The proposed new MARS is examined in experiments, in which a single UAV, dual UAVs, and combined UAV-UGV are tested in a research laboratory. The result indicates that the MARS can support automated path planning and indoor navigation for 2D imagery and 3D point cloud data collection.

Keywords: Building Automation, Sensory data collection, Multi-agent system, Robotics, Indoor inspection, Unmanned aerial/ground vehicle

1. INTRODUCTION

Facilities management plays an important role in maintaining the functionality of buildings [1, 2]. In practice, indoor inspection needs to be carried out regularly to avoid late identification of building defects, resulting in potential safety issues and economic loss [3]. Images and 3D point clouds are common data sources for indoor inspection. However, traditional data collection for indoor inspection relies on human inspectors, which is labor-intensive, time-demanding, and error-prone. Nowadays, automation and robotic technologies have gained attention due to their potential to reduce the workforce and time required to complete inspection tasks. Automation and robotic technologies with advanced sensing devices were applied for detecting and monitoring occupancy [4], floor cleaning [5, 6], fault detection and diagnosis [7], indoor air monitoring [8, 9], facility inspection [3], and construction site data collection [10, 11]. Early applications of robots focused on unmanned ground vehicles (UGV). The UGV-based approach provides greater efficiency and flexibility than manual solutions; however, UGVs are susceptible to obstacles in the inspection process [12]. Researchers have explored building-related inspection using unmanned aerial vehicles (UAV) to address this problem. Although UAVs are more agile and have better views than UGVs, they suffer from smaller payloads and shorter operational time [13]. Recently, there have been increasing amounts of studies on multi-robot systems, especially heterogeneous UAV-UGV systems, because the two types of robots can complement each other, improving the overall performance of the inspection [14].

Although multi-robot systems with UAV and/or UGV have been applied for various inspection tasks, there are still some limitations. First, automatic UAV-UGV systems are still lacking for indoor applications. In many studies, either UAV or UGV is controlled manually to move along a predefined path [15-17], which is not flexible enough for indoor navigation. It is necessary to develop new methods for UAV-UGV systems to navigate efficiently and automatically [10]. Secondly, conventional UAV-UGV systems may not be directly applicable to indoor environments. UGV may encounter obstacles, occlusions, or discrepant floor levels that prevent it from travelling into specified areas. In this case, UAVs can fly over the obstacles and move into the areas inaccessible by UGV. Thus, a collaboration between heterogeneous kinds of UGV and UAV devices can supplement each other for inspection in cluttered environments. This is evident in some previous studies wherein the view of the UGV is confined due to obstacles, and the UGV cannot navigate efficiently, which impacts the accuracy of collected data. UAV applications can assist the navigation of UGV by providing more accurate geometric information of the surrounding environment [18-20]. Furthermore, smaller-sized UAVs are often used indoors due to the confined space and safety considerations. Due to the small payload of lightweight UAVs, the sensor is usually a built-in camera, which can collect images and video clips. Using UAV alone might not be sufficient to carry larger scanning and sensing devices for managing the environmental data [10]. Developing a UAV-UGV system to leverage the strength of different robots for automated data collection is necessary.

This study aims to develop a multi-agent robotic system (MARS) for automating the collection of sensory data (such as images, video clips, and 3D point clouds) in cluttered environments. Firstly, a new architecture of MARS is developed for UAV/UGV indoor navigation and automated data collection. Following this, an enhanced shunting short-term memory (SSTM) model is developed to optimize path planning. Provided the optimized plan, UAV/UGV indoor navigation is assessed using simulation and LiDAR-based approaches. A coordinating control algorithm is proposed to promote the UAV-UGV coordination, including an information exchange mechanism. Finally, simulation and field experiments are conducted to demonstrate the feasibility and performance of the proposed MARS.

The main contributions of this paper are threefold. (1) A new system architecture of MARS is developed for automated sensory data collection in cluttered environments. Based on defined attributes and data requirement, functional modules for UAV, UGV, and mediating agent and their communication is constructed. UAV and UGV can exchange information via mediating agents for indoor navigation and sensory data collection (such as imagery data and point clouds) with this new system architecture. (2) An enhanced SSTM model is formulated to optimize the navigation path of UAV/UGV. This enhanced SSTM model can address multi-robot navigation issues by importing an inhibitory term resulting from robots. The computational complexity of this proposed method is not sensitive to the grid map size, so this method is advantageous over other conventional methods, especially in the cases where a larger grid size is used. (3) a coordinating control algorithm is proposed to enhance the coordination between UAV and UGV. UGV can request UAV’s assistance by sending messages to the mediating agent when it encounters obstacles based on the information exchange mechanism defined by the coordinating control algorithm. After receiving the commands from the mediating agent, UAV resolves the request by performing the corresponding task.

The rest of the paper is structured as follows. Section 2 reviews previous studies. Section 3 explains the proposed MARS system architecture and algorithms for UAV/UGV path planning and visual data collection. Section 4 presents simulation and experiment for multi-robot control with a single UAV, dual UAVs, and a combined UAV-UGV. Section 5 concludes the whole paper and discusses future work.

2. LITERATURE REVIEW

2.1. UGV for Indoor Applications

Rea and Ottaviano [21] developed a robotic inspection system using a hybrid structure of tracks and legs, where tracks were used to navigate, and legs were used to overpass obstacles. Various sensors were installed on the robotic platform to collect environmental data. The robotic platform was teleoperated by an inspector and provided limited support to automated inspection. Mantha et al. [22] tried to collect ambient data using a mobile ground robot that navigated based on fiducial markers. Compared with conventional data collection methods based on fixed stationary sensor networks, their approach is more effective and economical even though the system cannot actively avoid obstacles. Kim et al. [23] presented a new approach based on Robot Operating System (ROS) and Building Information Modeling (BIM), which assisted a robot in planning construction wall painting tasks. The authors have used BIM information and painting schedule to generate detailed elemental motions (e.g., grasping, moving, etc.) for the robot, which were then converted into control commands. The commands were finally sent to the robot through ROS to control the robot to perform the painting task. Yan et al. [7, 24] leveraged real-time heating ventilation air-conditioning operational data and generative adversarial network and practised automated fault detection and diagnosis (FDD) with robotic platforms. The fully automated FDD approach outperforms existing conventional heating ventilation air-conditioning FDD that uses semi-automated or supervised learning. However, previous relevant studies are mostly conducted in laboratory or simulation tests; a more practical approach verified in physical environments is needed. Besides, UGVs are inefficient when deployed in cluttered environments because UGVs (normally wheeled robots) can hardly access areas containing many obstacles and barriers [11].

2.2. UAV for Data Collection

To address the above issue, researchers have explored the application of UAVs in data collection within cluttered environments. For instance, Bolourian and Hammad [24] studied potential defect inspection for bridges using a UAV equipped with LiDAR. The authors have improved the inspection efficiency by optimizing the UAV's flight path, which was achieved by combining genetic algorithm and A* algorithm. Song et al. [25] proposed an automated approach for integrating LiDAR scanning and UAV. A set of waypoints were generated using greedy algorithm based on an occupancy map created using BIM data. The UAV moved to the waypoints for inspection using genetic algorithm and A* algorithm. Khosiawan and Nielsen [26] developed a UAV system with a scheduler for indoor monitoring and inspection. With the map, UAV status, and task information as the inputs, the scheduler can build an order of task execution for the UAV to navigate and inspect the environment in a time-optimized and anti-collision manner. Guerrero and Bestaoui [27] investigated structure inspection using UAVs, considering the influence of wind and energy limitations. They employed the genetic algorithm for path planning to minimize the time and energy required to complete the inspection. González et al. [28] tried to perform contact inspection using a LiDAR-equipped UAV. To improve the inspection efficiency, the authors have developed an iterative algorithm to plan the flight path of UAVs based on a voxel-based map. Likewise, Freimuth and Konig [29] performed construction inspections using UAV and BIM information. In this study, the inspection planner selected the expected inspection locations, followed by a UAV flying to the inspection locations using the A* algorithm. Although UAVs are more advantageous than UGVs in terms of agility and view, they have limitations such as smaller payload, shorter operational time, and safety issues.

2.3. UAV-UGV Collaborative Data Collection

Nowadays, multi-robot systems, which combine the strength of UAVs and UGVs, are gaining attention for data collection and other applications. Lakas et al. [30] developed a unified UAV-UGV framework for collecting data in the disaster-rescue scenario. In this system, UAV took ground images and created a map by recognizing road and obstruction features in the image data. The UGV navigated within the indoor environment based on the map information using the A* algorithm while collecting data for rescue tasks. Kim et al. [31] developed a UAV-UGV system for geometric data collection and 3D visualization, in which a UAV was deployed to collect images of a construction site to build its gradient-based map. The optimal stationary scanning positions were calculated with the gradient-based map, followed by the UGV navigating to these positions for collecting required data. Christie et al. [32] used a UAV and a UGV to estimate and confirm the locations of radiation sources. In their research, the UAV's task was to find the positions of radiation sources by flying over the area. Based on the position information, the UGV equipped with LiDAR promptly computed its movement path to determine the trajectory for radiation data collection. Kim et al. [33] developed a UAV-assisted automated framework for data collection in a cluttered environment. A UAV was first deployed to obtain an initial 3D map containing preliminary geometry information about a cluttered site. This map was then used to find the optimal scanning points by simulation. Finally, using the potential vector field method, the UGV moved to these scanning points to collect data for 3D mapping. Cantieri et al. [34] investigated power pylons using a cooperative UAV-UGV system, in which UGV served as a carrier of UAV to save battery while the UAV was used to perform the inspection tasks. The systems proposed in the previous relevant studies applied to outdoor environments require more research efforts on indoor applications.

In this sense, Michael et al. [15, 16] developed a UAV-UGV platform to cooperatively map the interior of a damaged building in the event of an earthquake. Firstly, a UGV was teleoperated to navigate and map the multi-floor environment. The operator controlled a UAV to perform the mapping when the UGV was inaccessible to a specified area. Their method increases the mapping efficiency and eliminates the risk of humans getting injured, but their system is still manually controlled. Mueggler et al. [17] demonstrated the collaboration of UAV and UGV in an indoor disaster scenario. A UAV took ground images at a predefined location based on a lawn-mower pattern, covering all areas. These images were then processed to create a map for the navigation of a UGV. The UGV navigated using the A* algorithm to collect information for a rescue mission. Although their system is effective and robust in a mock-up disaster scenario, the authors did not consider common and practical obstacles for UAV navigation. Harik et al. [35] developed a decentralised interactive architecture for UAV-UGV cooperation. With a broader view, UAVs can guide UGV's movement by scanning and providing images of the area around UGV. UGV navigated to the waypoints predefined by a human operator for data collection and inspection tasks. However, the drawback of their approach is that the system needs more human intervention. Qin et al. [36] designed a novel integrated vehicular system using collaborative UAVs and UGVs for exploration, mapping, and navigation in a GPS-denied environment. UGV performed a preliminary exploration using a view planning algorithm and produced a coarse map used as a fundamental model and a navigation reference for UAV. Then the UAV performed a fine complementary mapping using a tilting 2D laser module. The system has better environment perception and exploration efficiency, but its coordination scheme is not applicable for indoor data collection. Asadi et al. [10] developed an integrated UAV-UGV system to collect data at construction sites. By using a rapidly exploring random tree algorithm, a UGV navigated within a construction site while collecting data at the lower level. A blimp followed the UGV using a marker tracking technique while scanning the space at the upper level out of the UGV's view. Their developed system is automated, which is more efficient than the semi-automated ones, but their system is suitable for outdoor environment or spacious indoor environment, and not applicable for confined and cluttered indoor spaces because their UGV is designed for outdoor application [11] and their blimp is large. Besides, it does not consider obstacles for UAV navigation.

3. METHODOLOGY

Fig. 1 shows a schematic diagram of the proposed MARS. It starts by establishing (1) the system architecture, followed by (2) automated path planning and (3) indoor navigation and control. In Step 1, the system architecture defines the necessary attributes and data requirements for UAV/UGV and their connection with different sensing devices. A grid map is constructed to represent indoor spaces' geometric and obstacle features, then processed for path planning. In this study, path planning harnesses an enhanced SSTM model to generate the optimal movement trajectories for UAV and UGV in cluttered environments. Provided the optimized paths, Step 3 continues to verify the feasibility of the movement paths of UAV and UGV amid indoor navigation. Simulation-based approach and 2D LiDAR SLAM are leveraged to test the automated indoor navigation of UAV and UGV, respectively before real control is deployed for inspection. To accommodate the dynamic interaction between UAV and UGV, a mediating agent is developed and resolve the potential conflict and promote coordination for sensory data collection. The mediating agent encompasses a control algorithm and information exchange mechanism to interoperate UAV and UGV toward automated sensory data collection. The data collected by UAV/UGV are directly transmitted to and stored in the mediating agent for indoor applications. The methodology details are presented in the following sub-sections.

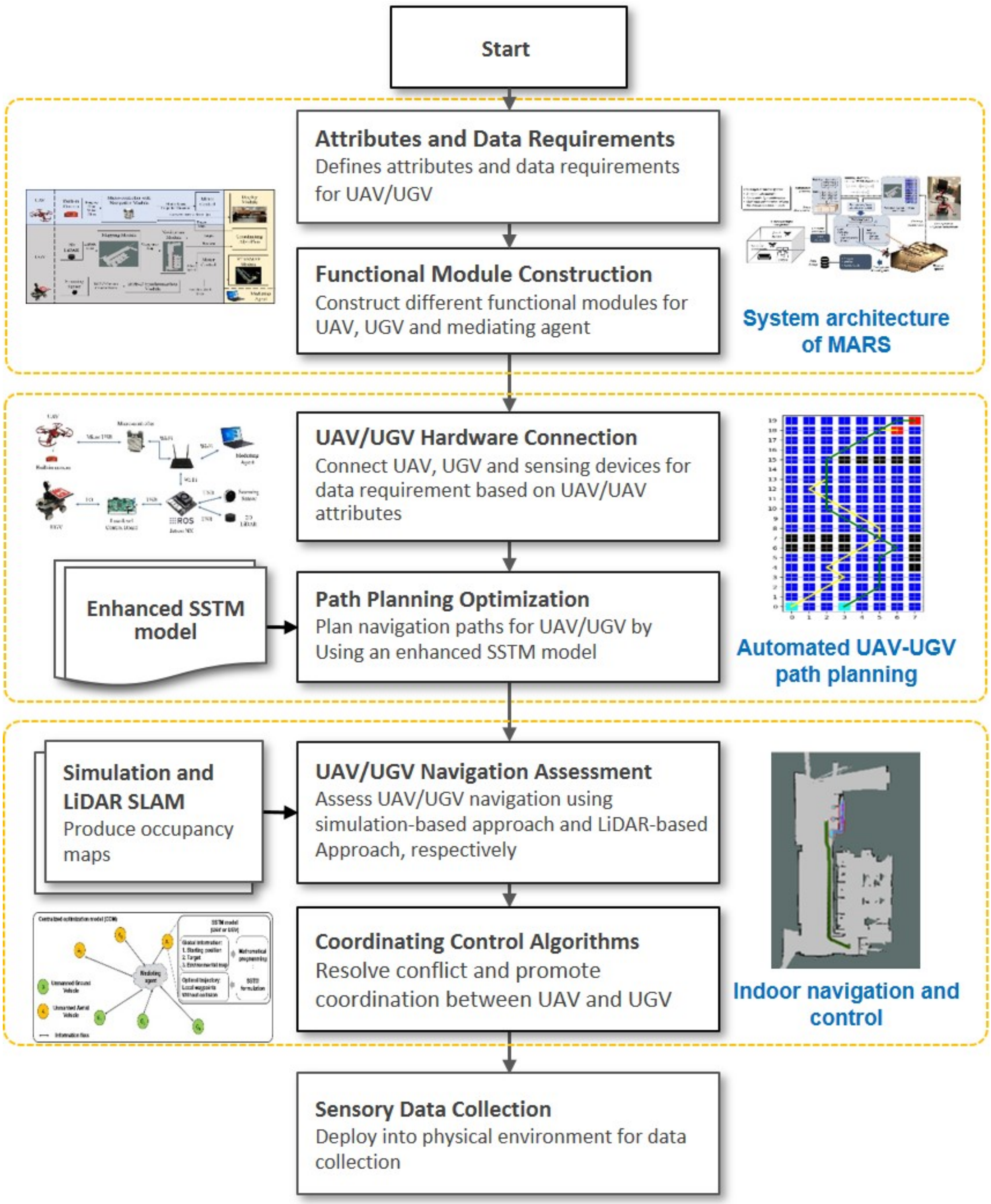

Fig. 1 Methodology framework of the proposed MARS

3.1. System Architecture of MARS

Fig. 2 illustrates the system architecture of MARS, which consists of three parts, namely UAV, UGV, and mediating agents connected via Wi-Fi. For UAV, its built-in camera collects the imagery data and video clips sent via a micro-controller to the display module in the mediating agent. Here, the mediating agent refers to a computing device that receives messages and processes the collected sensory data from UAV/UGV. Since UAV is subjected to a smaller payload, LiDAR can be hardly applied for its indoor localization and navigation. As such, a navigation module is developed in the micro-controller to compute and optimize the flight path of the UAV. Path planning optimization is conducted by an enhanced SSTM model for indoor navigation. The microcontroller then commands the UAV motor speed and propeller direction.

For UGV, there are two separate pipelines. In the first pipeline, UGV leverages a 2D LiDAR to scan and acquire 2D layout/geometry information of the surrounding environment. The layout information is sent to a mapping module wherein a 2D occupancy map (with a 5cm grid size) is generated. Provided the 2D occupancy map, the navigation module leverages SSTM to compute and optimize the path of UGV and then sends commands to control the UGV speed and movement. RGB-D images and camera poses are collected in the second pipeline by a scanning sensor fed into the RGB-D synchronization module (installed in a Jetson NX processor) to synchronize the imagery data into a single message. The message is sent to an RTABMAP module in the mediating agent to reconstruct the 3D point clouds of the indoor scene.

The mediating agent contains three modules: RTABMAP, coordinating algorithm, and display modules. First, the display module displays the imagery data and video streams from UAV. RTABMAP module is used to reconstruct the 3D point clouds using the RGB-D information collected by UGV. The mediating agent harnesses a coordinating algorithm to interoperate multiple UAV and UGV devices for data collection to improve inspection efficiency. For example, when UGV encounters an obstacle which prevents it from completing the data collection, its navigation module can communicate with the mediating agent by exchanging the target information and requesting the engagement of other devices in MARS (such as UAVs) for assistance. Details of the UGV, UAV and mediating agents are discussed in the following subsections.

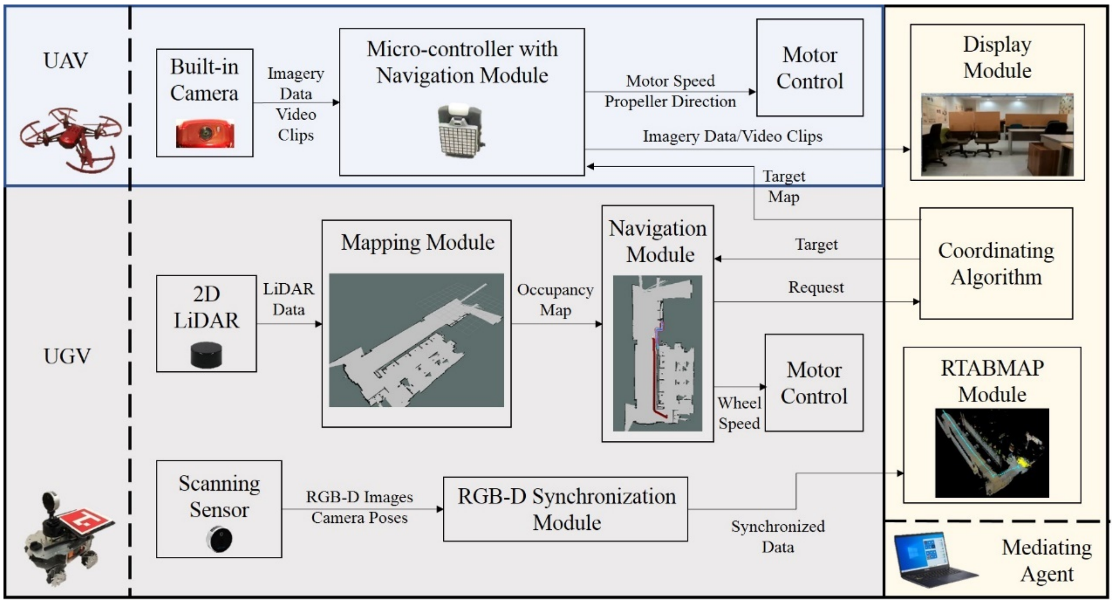

Fig. 2 System architecture for the proposed MARS

3.2. Automated UAV-UGV Path Planning

3.2.1. UAV and UGV

Fig. 3 displays the UAV and UGV used in this study. As shown in **Fig. 3 (a),** the UAV is a lightweight quadcopter including a built-in camera, four propellers, and an open-source micro-controller which supports aerial imagery collection. Such a lightweight quadcopter can reduce several safety issues and risks, such as flying into people, furniture, ceilings, or other objects. The micro-controller embeds with a Wi-Fi module that enables sending information remotely to the mediating agent. The camera can capture 5MP imagery data or live video clips sent to the mediating agent for storage. The open-source micro-controller is responsible for computational tasks (such as path planning) and supports the new application for algorithmic control of UAVs.

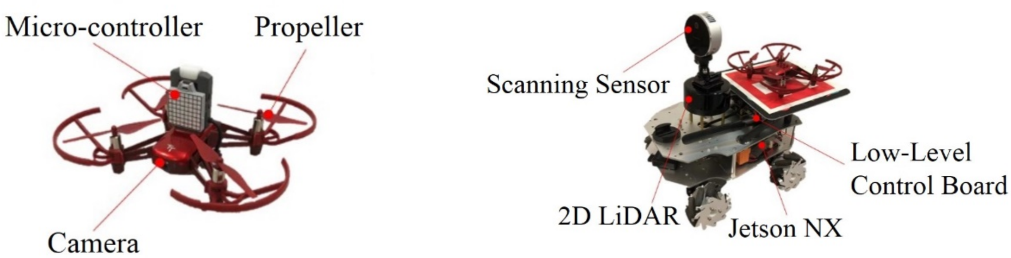

(a) UAV (b) UGV

Fig. 3 UAV and UGV used in this study

As shown in **Fig. 3 (b),** the UGV is a wheeled mobile robot with a Jetson NX processor, a control board, and multiple sensing devices for data collection. The Jetson

NX processor first executes the path planning optimization and determines the optimal path, which is sent to the low-level control board to move the UGV around indoor spaces. Sensing devices include a 2D LiDAR that acquires the space layout information for 2D mapping and indoor navigation. In addition, a scanning sensor is used to collect RGB-D images and camera poses for generating 3D point clouds and reconstructing the 3D scene. Specifically, the Jetson NX processor is used to exchange RGB-D information with the mediating agent (via Wi-Fi) for generating the 3D point clouds. **Fig. 4** illustrates the 3D point cloud reconstruction process using RTABMAP. RTABMAP has been integrated into the Robot Operating System (ROS), where data processing units are presented in the form of nodes. RTABMAP-based 3D reconstruction involves five nodes: sensor, RGB-D synchronization, RGB-D odometry, rtabmap, and rtabmapviz. The sensor node controls the scanning sensor to collect RGB-D images for the surrounding environment and camera poses, then synchronized in the RGB-D synchronization node. Following this, the synchronized data is sent via Jetson NX processor to the RGB-D odometry node (in the mediating agent), where odometry data are derived by computing the transformation between two consecutive RGB-D image pairs using the RANSAC approach. Then, the Rtabmap node takes RGB-D images, camera poses, and odometry data to produce 3D point clouds using RTABMAP with the aid of an incremental appearance-based loop closure detector. Finally, the 3D point clouds, RGB-D images, and odometry data are integrated into the rtabmapviz node for 3D scene visualization. The main task of the UGV is to collect imagery data and point clouds in most areas, because UGV can be equipped with more sensors and works for a longer time. In addition, the UGV can serve as a carrier/platform for the UAV.

Fig. 5 shows the connection between UAV, UGV, sensing devices, and the mediating agent in this study. UAV and UGV are connected to the mediating agent via Wi-Fi created by a router. The sensing devices, motors, and miscellaneous processors (i.e., micro-controller, low-level control board, and Jetson NX) are connected via USB and I/O cables.

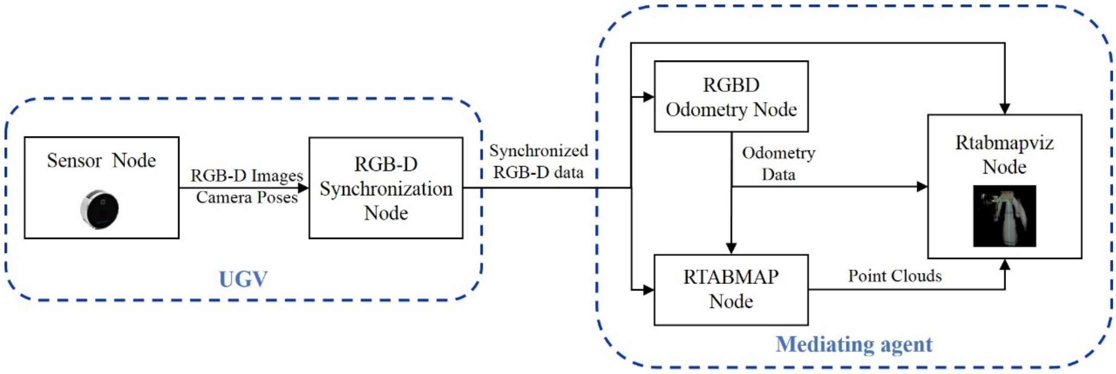

Fig. 4 3D point cloud scene reconstruction process using RTABMAP

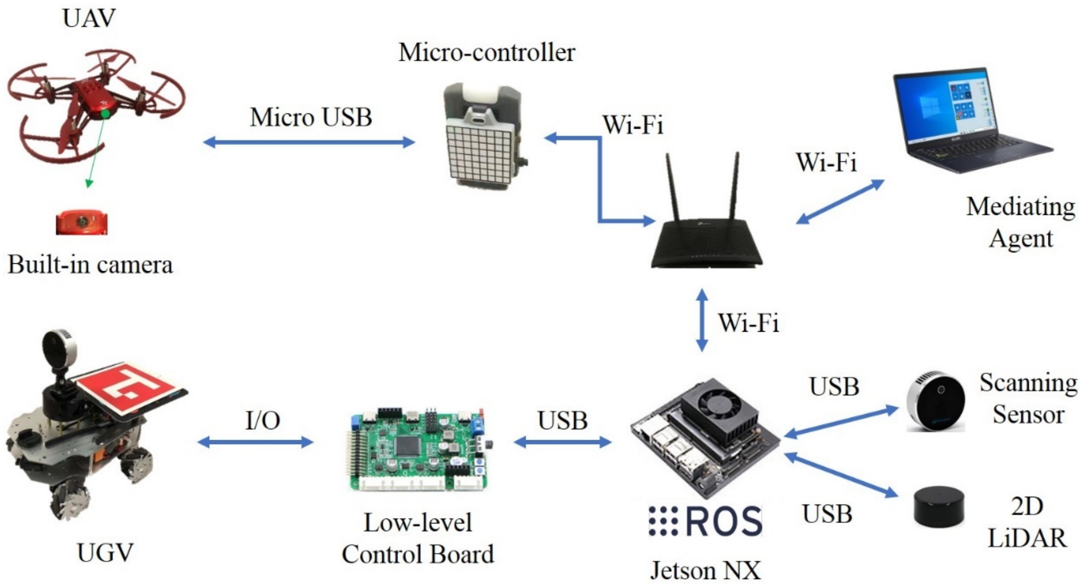

Fig. 5 Connection between UGV, UAV and sensing devices

3.2.2. Path Planning Optimization

To enhance the efficiency of data collection in cluttered environments, efficient indoor navigation is necessary. Therefore, indoor path planning optimization is a central task. This paper develops an enhanced SSTM model to generate the optimal paths for UAV and UGV movement without colliding with obstacles and other devices that work in the same environment [37]. The original SSTM model is inspired by Hodgkin and Huxley's study on the dynamics of voltage across the membrane [38], Grossberg's shunting model [39], and the neural network dynamics model for path planning proposed by Glasius et al. [40]. The application of the SSTM model is built on the construction of neural network architecture, as shown in **Fig. 6.** The whole neural network represents a finite-dimensional (F-D) configuration space Θ of a robot. For example, Θ can refer to a 2-D Cartesian workspace for a point robot that moves in a 2-D space. For a point robot that navigates in a 3-D space, Θ stands for the 3-D Cartesian workspace. The location of one neuron in the network, denoted by a vector $p_i \epsilon R^F$, is one element in Θ. Each neuron can interact with its neighboring neurons locally. The range in which this interaction can occur is called the neurons' receptive field in the neurophysiology [41]. Since it was first proposed, the SSTM model has been applied to various path planning research [42-44].

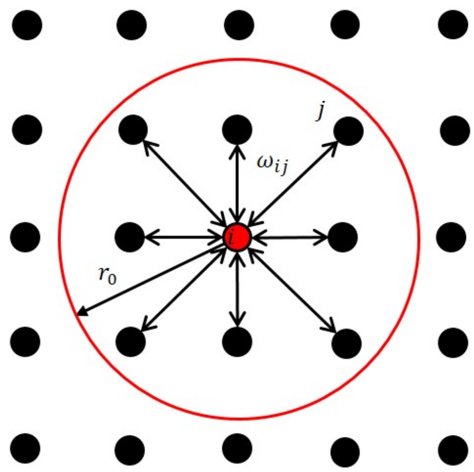

Fig. 6 Schematic diagram of the neural network in SSTM

According to [45], the dynamics of i^{th} neuron are modeled mathematically by a shunting equation, as shown in Eq. (1) below:

$$\frac{dx_i}{dt} = -Ax_i + (B - x_i)\left([I_i]^+ + \sum_{j=1}^{k} \omega_{ij}[x_j]^+\right) - (D + x_i)[I_i]^- \tag{1}$$

wherein x_i denotes the neural activity of i^{th} neuron; x_j denotes the neural activity of the neighboring neurons of i^{th} neuron; k denotes the number of the neighboring neurons; A, B and $-D$ are the passive decay rate, upper and lower bounds of the neural activity, respectively. A, B and D are all positive constants. ω_{ij} denotes the connection weight between i^{th} and j^{th} neurons; $[I_i]^+ + \sum_{j=1}^{k} \omega_{ij}[x_j]^+$ and $[I_i]^-$ are the excitatory and inhibitory inputs for i^{th} neuron. ω_{ij} is defined as follows:

$$\omega_{ij} = f(|d_{ij}|) \tag{2}$$

wherein d_{ij} represents the Euclidean distance between i^{th} and j^{th} neurons and is calculated as $p_i - p_j$.

Considering that i^{th} neuron can only be influenced by its neighboring neurons within the receptive field, function $f(a)$ has the property of decreasing monotonically and can be defined as follows.

$$f(a) = \begin{cases} \frac{\mu}{a}, & if\ 0 < a < r_0 \\ 0, & if\ a \geq r_0 \end{cases} \quad (3)$$

wherein r_0 refers to the distance of the receptive field, which has a positive value and μ is a positive constant according to the specific cases.

The excitatory input results from the target and lateral connections among neurons, while the inhibitory input results from the obstacles only. Functions $[a]^+$ and $[a]^-$ can be defined as follows:

$$\begin{cases} [a]^- = max\{-a, 0\} \\ [a]^+ = max\{a, 0\} \end{cases} \quad (4)$$

I_i is defined as shown in Eq. (5):

$$I_i = \begin{cases} E, & if\ it\ is\ a\ target \\ -E, & if\ it\ is\ an\ obstacle \\ 0, & otherwise \end{cases} \quad (5)$$

wherein E is a very large positive constant, $E \gg B$. Based on the SSTM model defined in Eq. (1), the positive neural activity can propagate over the whole neural network through local interaction. The negative neural activity stays locally at the neurons representing obstacles. By such a definition, a robot is globally attracted to the target, while the obstacles have a local effect to expel the robot [46].

The dynamic activity landscape of the neural network then produces a navigation path for the robot according to the deepest gradient ascent. Assuming the location of the neuron in which the robot lies currently as p_c, the location of the neuron that the robot would move toward can be derived as follows:

$$p_{next} \leftarrow x_{p_{next}} = \max_{j=1,2,\ldots,k}\{x_j\} \quad (6)$$

wherein p_{next} denotes the next position (neuron) where a robot chooses to move toward; $x_{p_{next}}$ denotes the neural activity of the next position (neuron); x_j denotes the neural activity of the neighboring neurons of the current position (neuron); k is the number of the neighboring neurons. Based on Eq. (6), the robot keeps moving from the current position to the next position until it reaches the target.

However, the original SSTM model cannot ensure collaborative motion for multiple robots and prevent one robot from running into other devices, especially in cluttered environments. This issue is illustrated in in **Fig. 7 (a)**, where Robots 1 and 2 are present in red and blue neurons respectively. Assuming that the three yellow neurons between Robots 1 and 2 are closer to the target, the neural activity for these yellow neurons would be relatively larger according to the formulation of the original SSTM. In such a case, Robots 1 and 2 have large possibilities to simultaneously move to the same yellow neuron, resulting in collision. To deal with this issue, our enhanced SSTM introduces an inhibitory term $\sum_{j=1}^{m} \widetilde{\omega}_{ij} C_j$ to cater for the impact from multiple devices, as follows.

$$\begin{aligned} \frac{dx_i}{dt} = -Ax_i + (B - x_i)\left([I_i]^+ + \sum_{j=1}^{k} \omega_{ij} \left[x_j\right]^+ \right) \\ - (D + x_i)\left([I_i]^- + \sum_{j=1}^{m} \widetilde{\omega}_{ij} C_j \right) \end{aligned} \tag{7}$$

wherein x_j denotes the neural activity of the neighboring neurons of i^{th} neuron; m is the number of the neighboring neurons representing robots (which is called robot neuron in this paper); C_j denotes the negative impact rate by j^{th} robot neuron, which is a negative constant; $\widetilde{\omega}_{ij}$ denotes the connection weight between i^{th} neuron and j^{th} robot neuron. $\widetilde{\omega}_{ij}$ and I_i are defined as shown in Eqs. (8) and (9) below:

$$\widetilde{\omega}_{ij} = \beta \omega \tag{8}$$

$$I_i = \begin{cases} E, & if\ it\ is\ a\ target \\ -E, & if\ it\ is\ an\ obstacle \\ C, & if\ it\ is\ a\ robot \\ 0, & otherwise \end{cases} \tag{9}$$

in which β is a positive constant, $\beta \in [0,1]$. E and C are very large positive constants, $E \gg B$ and $C \gg B$. The neural activity of each neuron is updated according to Eq. (10) by the first-order approximation equation of Taylor's theorem:

$$x_i(t + \Delta t) = x_i(t) + \frac{dx_i(t)}{dt} \cdot \Delta t \tag{10}$$

in which $x_i(t)$ is the neural activity of i^{th} neuron at time t; Δt is the interval between two consecutive updates.

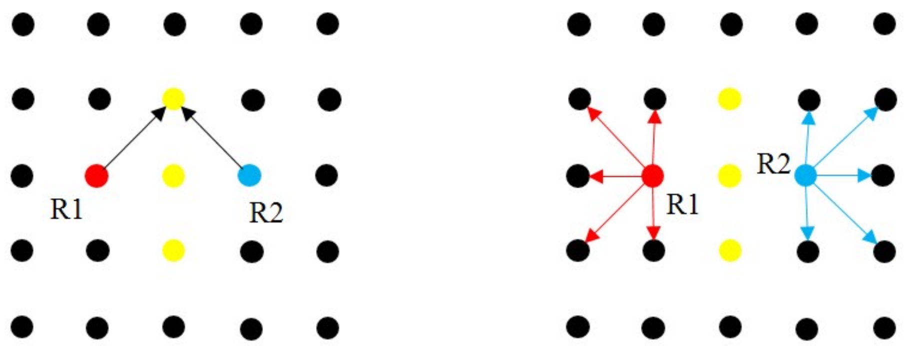

(a) Original SSTM Model (b) Enhanced SSTM Model

Fig. 7 Illustration of robotic motions before and after using the enhanced SSTM

As shown in **Fig. 7 (b)**, based on the enhanced SSTM, Robot 1 and Robot 2 have negative impacts on the yellow neurons, which reduces their neural activities. This indicates that Robot 1 would have a higher possibility or priority to move to the other five neighboring neurons (highlighted by red arrows) rather than the yellow neurons. Similarly, Robot 2 has less possibility for moving into the yellow neurons, which is illustrated by blue arrows. As a result, the potential collision between multiple devices can be resolved.

The enhanced SSTM model addresses local connections between the neighboring neurons, so that the computational complexity and time depend linearly on the neural network size. As such, the enhanced SSTM does not require a computationally demanding learning process in practices. It can be more conveniently leveraged to promptly optimize the path planning and control the UGV/UAV for data collection in cluttered environments. In addition, our enhanced SSTM can demonstrate better performance over conventional methods, because it is less sensitive to the grid map size. Specifically, a finer grid is often used to generate more accurate paths in cluttered environments, indicating that the grid map size can be larger. In this study, only 2-D Cartesian workspace is considered, and one neuron in the neural network corresponds to one position on 2D planar space. The grid map is designed based on 2D planar space so that the neural network size is equal to the grid map size. As a result, the computational time depends on the grid map size, which can be represented by $O(n)$ and n is the grid map size. Increases in the grid map size does not substantially increase the computation time, which is the strength of the SSTM for indoor path planning and navigation. Furthermore, the optimized path based on the enhanced SSTM represents the global optimum, which is another advantage as compared with Dijkstra and A* Algorithms that may be constrained in local optimum.

3.3. Indoor Navigation and Control

3.3.1. UAV/UGV Indoor Navigation

Provided the path planning, this section continues to explain the UAV-UGV navigation and control. For UAV, the indoor space needs to be modeled as a grid map for assessing the feasibility of the optimized flight path. **Fig. 8** shows the procedure of modeling the indoor space. Firstly, 3D mapping is conducted based on the configuration of the indoor space. Secondly, the 3D mapping is converted into a 2D grid map assuming that UAV is operated at the same height level within the indoor space. Finally, an occupancy map can be built by assigning obstacle features to the 2D grid map. To achieve better obstacle avoidance, this study defines the size of a grid to be larger than that of UAV. In the 2D occupancy map, an occupied grid highlighted in black represents an obstacle. **Fig. 8** demonstrates how to decide an occupied grid. A grid that is occupied partially or entirely by an obstacle is treated as a fully occupied grid to facilitate the computation. Regarding the flight pattern of UAV on the grid map, UAV can move only from the center of one grid to the center of the adjacent grid (see **Fig. 9)**. UAV is not allowed to stop on the edge or boundary of any grid cells. Besides, it can only move in eight directions, namely up, down, left, right, up-right, up-left, down-right, and down-left. By running a UAV simulation based on the optimized path from the enhanced SSTM, the feasibility of the flight trajectory can be verified.

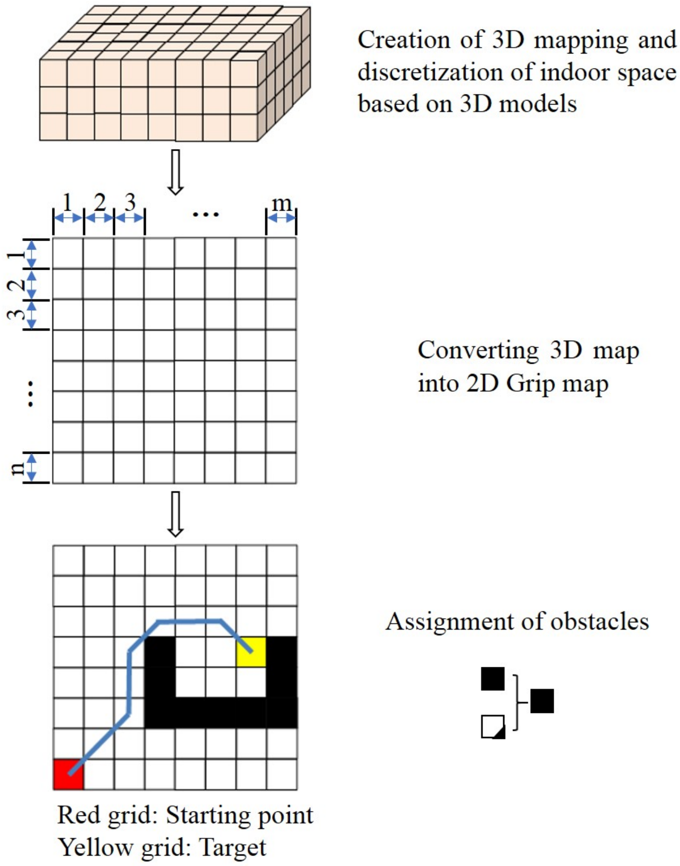

Fig. 8 Procedure of modeling indoor spaces for UAV

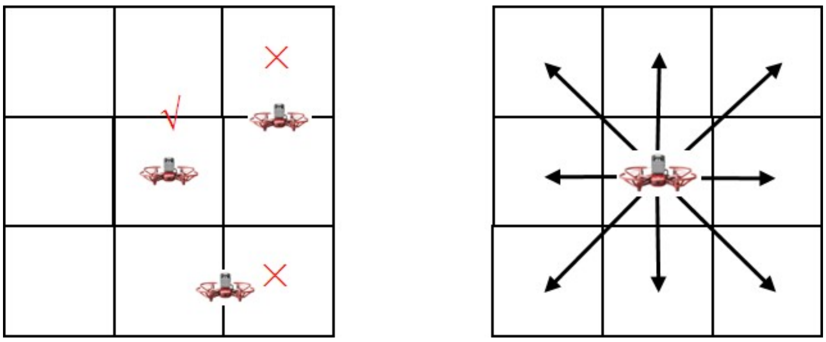

Fig. 9 Flight pattern of UAV on the grid map

Fig. 10 shows the assessment of indoor navigation for UGV by a LiDAR-based approach in ROS. The first step is to build an occupancy map of the indoor environment using 2D LiDAR and SLAM algorithm. Point clouds from 2D LiDAR are collected and registered first using an iterative closest point algorithm. Then, the SLAM algorithm estimates the UGV pose and obstacle location by matching the 2D point clouds. At the same time, one or more loop closures may be identified and established during the UGV movement. The SLAM algorithm utilizes the loop closure information to update the occupancy map (with 5cm grid size). Provided the occupancy map, the enhanced SSTM computes the optimal movement path for UGV. Adaptive Monte Carlo localization algorithm is used to generate the positioning information for UGV. Based on the movement path and positioning information, UGV can navigate from the starting point to the target.

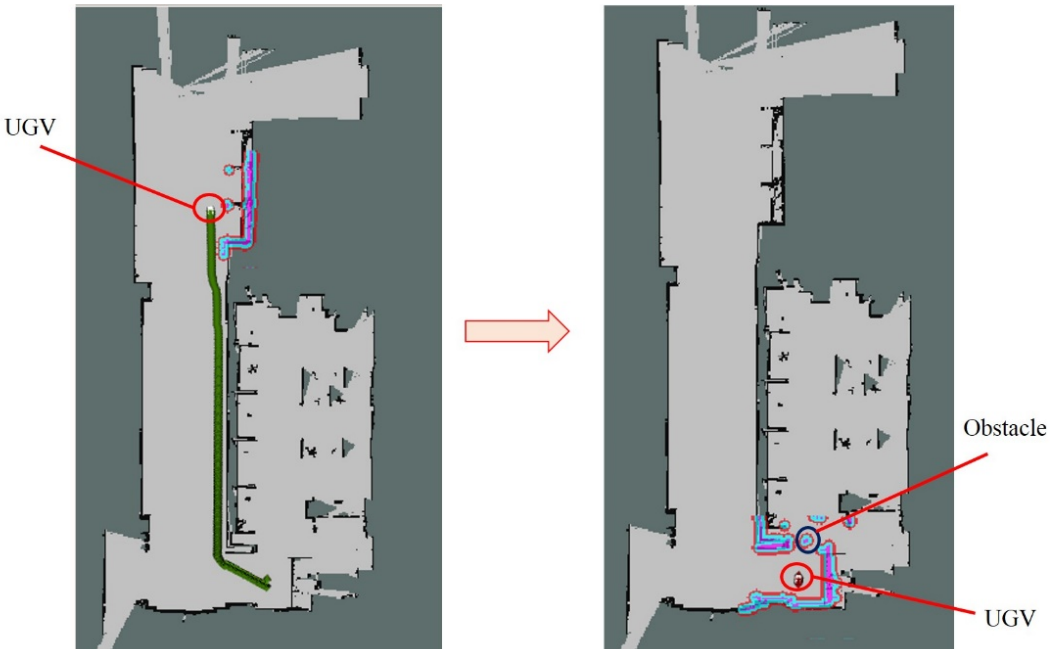

Fig. 10 UGV navigation with 2D LiDAR SLAM

3.3.2. Coordinating Control Algorithms

After the optimized path for UAV/UGV are tested and verified, the logical routines for UAV and UGV can be formulated to support automated control. As shown in **Fig. 11**, to accommodate the dynamic interaction and conflicts between UAV and UGV, the mediating agent harnesses a coordinating control algorithm to resolve the potential conflict and promote coordination between UAV and UGV for sensory data collection. The core of the mediating agent lies in the efficient control algorithm that is constructed to define the information exchange mechanism including message type, sender, receiver, timestamp to guarantee the seamless data exchange amongst UAV and UGV. As such, it interacts with UAV/UGV to obtain necessary information such as indoor scenes, obstacles, and data collection tasks. With the provided information, the mediating agent intends to coordinate UAV and UGV iteratively by generating a set of logical sequences and decision routines. Such a logical sequence can be executed for controlling the UAV and UGV in the physical environment.

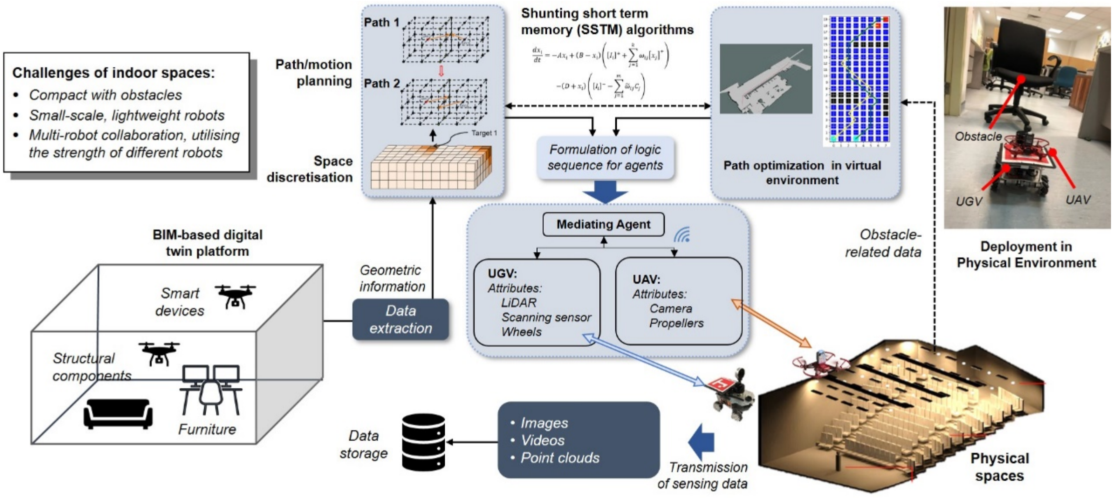

Fig. 11 Coordinating control and information exchange for UAV and UGV

The mediating agent communicates with UAV/UGV by employing the SOCKET interface which contains two types of communication protocols, i.e., Transmission Control Protocol (TCP) and User Datagram Protocol (UDP). TCP is more reliable and accurate in term of data transmission, so it is used to send control-related information or receive the information from UAV/UGV. UDP requires less time to process packets, and makes more efficient use of bandwidth, thereby it is used to receive sensing data such as imagery data and video clips. Such a configuration can achieve the best trade-off between the efficiency and reliability of data transfer.

A generic form of the message is constructed as *messageType (sender & receiver)* and *messageContents,* where *messgeType* and *messageContents* are specific to the stage of the coordination process. The *sender* and *receiver* correspond to the index of the agent that sends and receives the message, respectively. **Fig. 12 (a)** demonstrates the information exchange mechanism in the control algorithm. In general, UAV and UGV perform different tasks because of their distinct characteristics. The mediating agent serves as the central authority to coordinate UAV and UGV iteratively to perform complicated tasks. **Fig. 12 (b)** shows information exchange process in the proposed MARS. The information exchange includes five major steps.

i. First, mediating agent receives affair (Q) from a UGV. In this context, the UGV is the message sender and initiates the resolution process by sending the affair message (such as facing an obstacle) to the mediating agent.
ii. Upon receiving the affair message, the mediating agent starts announcing the affair (Q) and seeking other devices such as UAVs for assistance and

resolution of the affair encountered by UGV.

iii. UAVs send messages regarding their current positions (P_i) to the mediating agent. According to the affair (Q) and the current positions of UAVs (P_i), the mediating agent weighs their availabilities and eligibilities (W_i).

iv. The mediating agent prioritizes UAVs based on the nature of the affair and position information. Afterwards, the mediating agent announces an award message to the selected UAV with the highest priority.

v. The selected UAV helps resolve the affair (e.g., replace UGV to continue the inspection task). On receiving the award message, the selected UAV continues to complete its current inspection task. Upon the completion of the current inspection, UAV then re-optimizes its path planning to assist the UGV for inspection. The coordination terminates when the selected UAV finishes the new task.

(a)

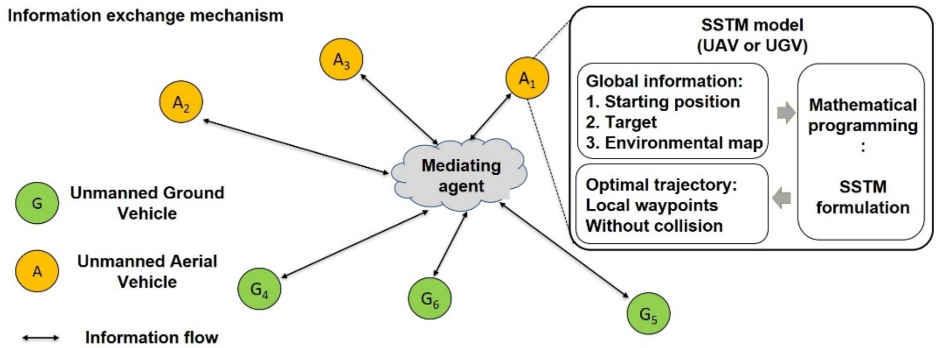

(b)

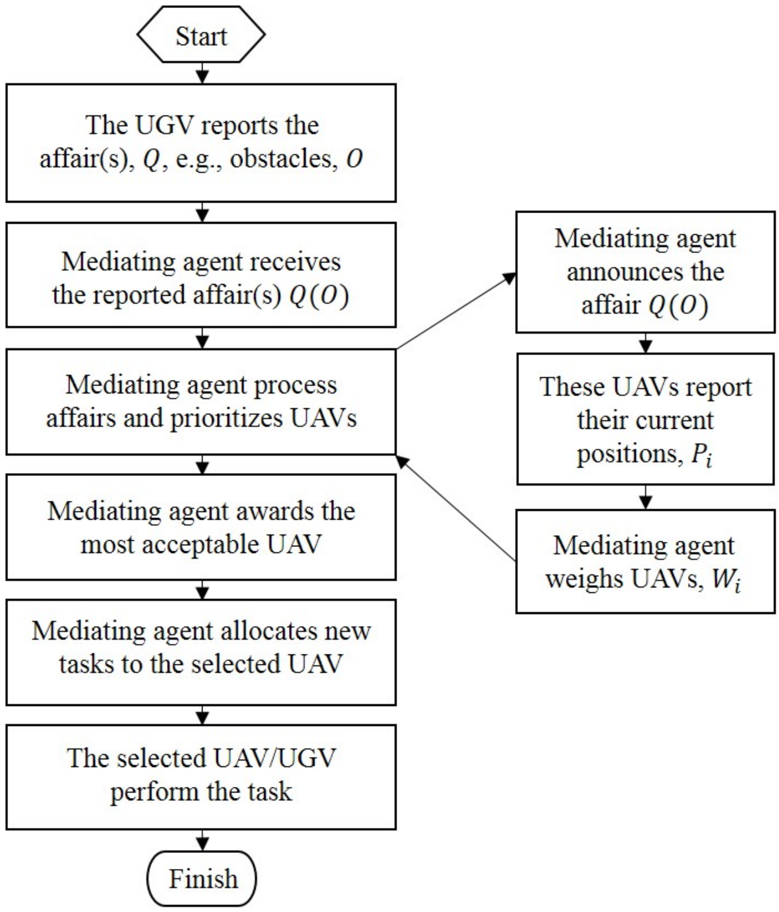

Fig. 12 Information exchange mechanism for the coordination algorithms

Fig. 13 shows the pseudo-code that explains the logical sequence for path planning of a single UAV taking account of the information exchange with a mediating agent. The algorithm requires a starting point, a target position, and an initial number of time steps for calculating the initial neural activity. To begin with, the neural network is constructed and initialized according to the grid map of an indoor space, in which the neural activity of the target neuron is assigned as one, whereas other neurons are set as zero. Before the UAV flies, the neural activities are promptly updated to generate a larger gradient for neurons near the starting point. This is because neurons near the starting point are usually far from the target and have neural activities of zero. Therefore their neural activities require multiple updates to generate a larger gradient for the UAV to determine its movement. A larger gradient of neural activities helps UAVs to navigate more easily. With a grid map represented by different neural activities, UAV starts to move around the indoor space to collect the imagery data.

The UAV progressively checks the position of the current neuron, and if its current neuron reaches the target, the inspection task is completed. Otherwise, UAV attempts to find and move to the next neuron with the largest neural activity by exploring and comparing the value of its current neuron with neighboring neurons. After UAV arrives its next neuron, the neural network is updated. This process iterates until the UAV arrives at the target. During its flying process, the built-in camera of UAV records the condition of surrounding facilities and indoor spaces by taking images or video clips, which are sent to the mediating agent through UDP.

When it receives an affair message from the mediating agent, the UAV reports its current position (P_i). Based on the current grid map (G_E) and target position $P_t = (x_t, y_t)$, the mediating agent weighs the current position of UAV (P_i) and its eligibilities (ω_i), which are used to assign the new inspection task. After UAV completes the current inspection, the UAV can leverage the new grid map ($G_E{}'$) and target $P_t{}'$ to generate the new waypoints (using enhanced SSTM) and compute the corresponding neural network for navigation. The control algorithm for dual UAVs is similar to that of a single UAV, except that there are two starting points, two targets, and two neural networks. Updates of neural activities are performed according to the enhanced SSTM model in this paper to avoid potential collision in cluttered environments. **Fig. 14** describes the pseudo-code for dual UAVs, which explains its procedures explicitly.

Algorithm 1 Pseudo-code for Path Planning of UAV

```
This algorithm aims for path planning of a single UAV
Procedure:
Input: Starting position (x_s, y_s)
Input: Target: (x_t, y_t)
Set: The initial number of time steps each of which is time interval Δt
Initialize: Neural network
repeat
    for Each time step do
        Update the neural activities of the neural network
    end for
until it reaches the predefined initial number
UAV starts to work from the starting position
for UAV do
    Obtain its current neuron
    if its current neuron is NOT the target then
        Compare the neural activities of its neighboring neurons
        Find the neuron with the largest neural activity
        Move to that neuron while taking videos of the environment
        Update the neural activities of the neural network
    end if
    if receiving affair(s) message Q from the mediating agent then
        Report the updated position (x_i, y_i)
```

end if
if receiving an award announcement from the mediating agent **then**
  if it finishes its current task **then**
    Start to perform the task allocated by the mediating agent
  else
    Stores the task allocated by the mediating agent
  end if
end if

Fig. 13 Proposed SSTM algorithm for path planning of UAV considering the information exchange with the mediating agent

Algorithm 2 Pseudo-code for Dual UAVs Path Planning

This algorithm aims to coordinate two UAVs in a sense that they can navigate without colliding with obstacles and the other UAV
Procedure:
Input: Starting position (x_{s1}, y_{s1}), (x_{s2}, y_{s2})
Input: Target: (x_{t1}, y_{t1}), (x_{t2}, y_{t2})
Set: The initial number of time steps each of which is time interval Δt
Initialize: Neural network
for Each UAV **do**
  repeat
    for Each time step **do**
      Update the neural activities of the whole neural network
    end for
  until it reaches the predefined initial number
end for
UAV starts to work from the starting position
for Each UAV **do**
  Obtain its current neuron
  if its current neuron is **NOT** the target **then**
    Compare the neural activities of its neighboring neurons
    Find the neuron with the largest neural activity
    Move to that neuron while taking videos of the environment
    Update the neural activities of the neural network
  end if
end for

Fig. 14 Proposed SSTM algorithm considering the coordination of dual UAVs

4. EXPERIMENT

4.1. Experimental Environment

To elaborate the proposed MARS, field experiments are conducted on the construction technology laboratory at National University of Singapore. **Fig. 15** shows the 3D model, layout plan, picture, and occupancy map of the laboratory. Three different scenarios are tested separately, which are single UAV, dual UAVs, and combined UAV-UGV for data collection.

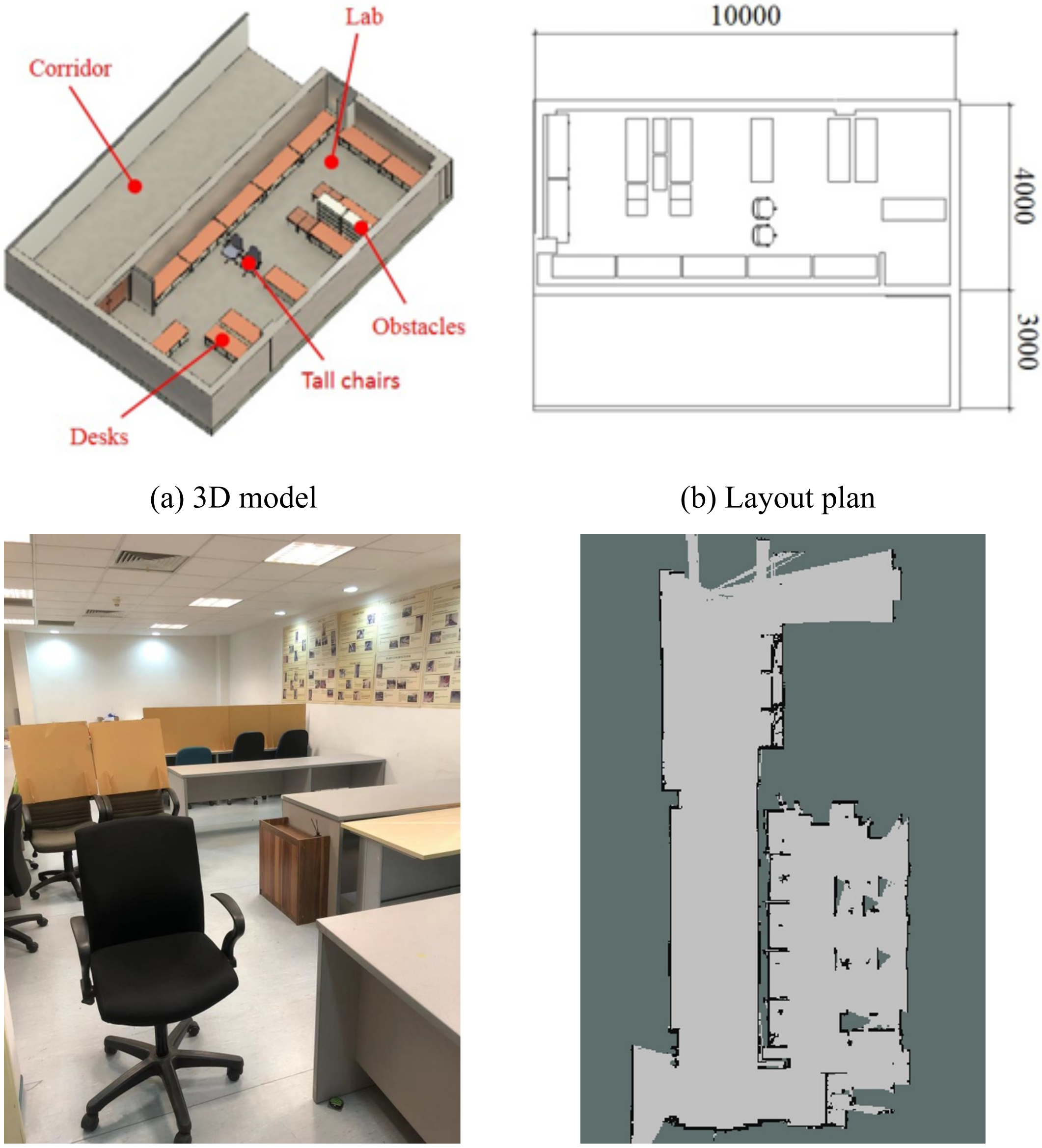

(a) 3D model (b) Layout plan

(c) Real scene (d) Occupancy map

Fig. 15 Overview of the Construction Technology Laboratory

4.2. Indoor Navigation for Single UAV

The UAV used in the experiment is DJI Robomaster TT. The overall size of the grip map for UAV is four meters (width) and ten meters (length). The size of each grid is set as one meter. Such a grid map reduces the computational time required for simulation while achieving satisfactory accuracy of path planning. The neural network is constructed as a 4×10 grid, where the neural activities for all the grids are assigned as zero except that the target is set as one. Parameters of the enhanced SSTM model are defined for path planning optimization (i.e., $A = 20$, $B = 1$, $D = 1$; $\mu = 0.7$, $\beta = 1$ for lateral connection; $E = 50$ for external inputs; $C = 20$ for added inhibitory term; and $\Delta t = 0.01$ for the interval of updating). The simulation result is shown in **Fig. 16**. The blue grids are free spaces where the UAV can move freely. The dark, light blue and red grids represent obstacles, starting position, and target, respectively. There are three alternative shortest paths from the starting position to the target without collision, which are denoted as Paths 1, 2, and 3 in **Fig. 16**. While all the three paths are the optimum, Path 1 is selected as the navigation trajectory for the UAV to move to the target.

To demonstrate the feasibility of indoor navigation, a field experiment is conducted. **Fig. 17** shows the flight trajectory of UAV (highlighted by a red polyline in the 3D model) and the real-time imagery data and video clips collected by the UAV. The UAV automatically flies from the starting position to the target and avoid all the obstacles in compliant with the optimized Path 1 (in **Fig. 16**), which is derived from the enhanced SSTM. The results indicate that the proposed MARS can satisfactorily generate an optimal flight path for UAV to move and collect imagery data within a cluttered environment which contains many obstacles.

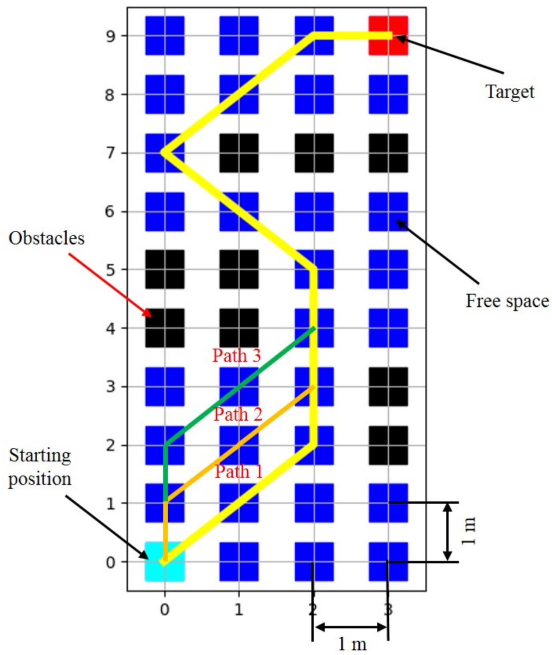

Fig. 16 Path planning for a single UAV

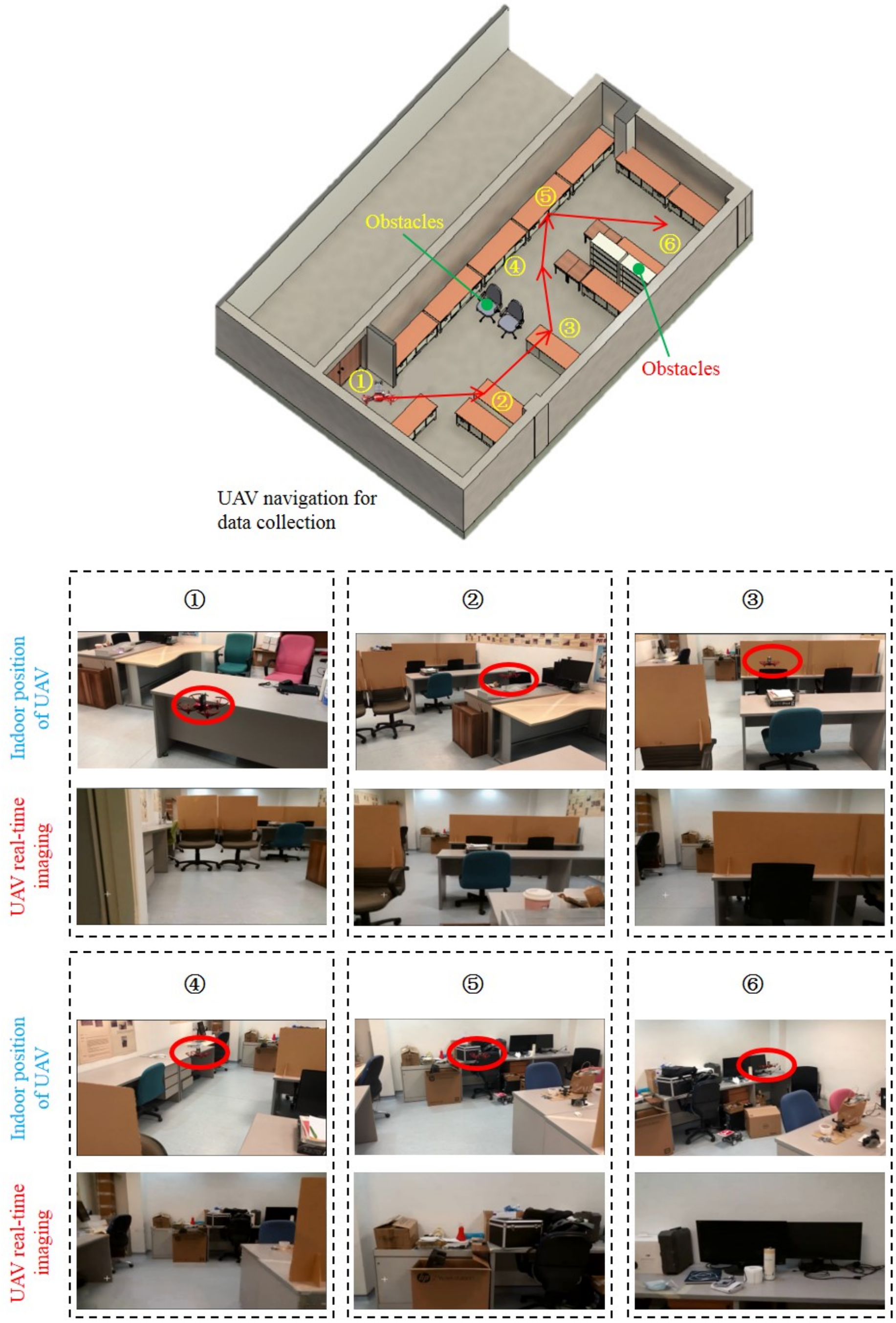

Fig. 17 Indoor navigation and data collection of a single UAV

4.3 Indoor Navigation for Dual UAVs

In the second experiment, dual UAVs are tested on an 8×20 grid map and the grid size are 50×50 cm. Based on the created grid map, the neural network is constructed with the same configuration containing 8×20 neurons. The parameters of the enhanced SSTM are defined to support path planning of dual UAVs (i.e., $A = 50$, $B = 1$, $D = 1$; $\mu = 0.7$, $\beta = 1$ for lateral connection; $E = 100$ for external inputs; $C = 20$ for added inhibitory term; and $\Delta t = 0.01$ for interval of updating). To verify that our enhanced SSTM has advantages for multi-robot path planning, another simulation using the original SSTM model is carried out. **Fig. 18 (a)** and **Fig. 18 (b)** show the path planning results using original and enhanced SSTM models, respectively.

As shown in **Fig. 18 (a)**, the two UAVs may collide during t_5-t_7 when UAV1 flies from $(4,4)$ to $(5,5)$ and UAV2 flies from $(5,4)$ to $(4,5)$. Since the UAVs fly at the same height level, they have a high possibility to collide with each other. The same problem occurs when UAV1 flies from $(5,5)$ to $(4,6)$ while UAV2 flies from $(4,5)$ to $(5,6)$. The results indicate that the original SSTM model cannot guarantee a safe indoor path planning and navigation for multiple devices in cluttered environments. **Fig. 18 (b)** shows the results generated from the enhanced SSTM. UAV1 moves from its starting position $(0,0)$ to the target $(6,18)$, following its optimized trajectory highlighted in yellow polyline. UAV2 starts from $(3,0)$ and follows an alternative trajectory (green polyline) to the target $(7,19)$. Both UAVs do not run into obstacles in the laboratory. In the 2D grid map, their flight paths are overlapped at coordinates $(5,7)$, $(2,11)$, $(2,13)$, $(2,14)$, $(2,15)$, $(3,16)$, $(4,17)$, and $(5,18)$. However, these do not imply any collisions because UAV1 and UAV2 arrive on these positions at different time steps, as shown in the table of **Fig. 18 (b)**. The comparative analysis also proves that our proposed mathematical formulation to SSTM model is necessary and useful to cater for multi-robot indoor navigation.

(a)

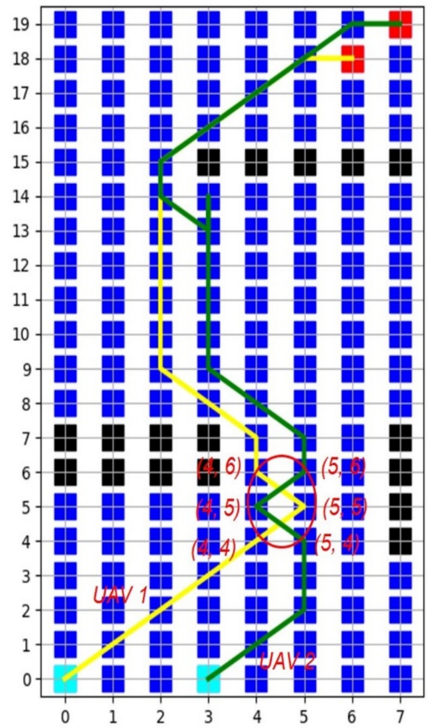

Time steps	UAV 1	UAV 2
t_1	(0,0)	(3,0)
t_2	(1,1)	(4,1)
t_3	(2,2)	(5,2)
t_4	(3,3)	(5,3)
t_5	(4,4)	(5,4)
t_6	(5,5)	(4,5)
t_7	(4,6)	(5,6)
t_8	(4,7)	(5,7)
t_9	(3,8)	(4,8)
t_{10}	(2,9)	(3,9)
t_{11}	(2,10)	(3,10)
t_{12}	(2,11)	(3,11)
t_{13}	(2,12)	(3,12)
t_{14}	(2,13)	(3,13)
t_{15}	(2,14)	(3,14)
t_{16}	(2,15)	(3,13)
t_{17}	(3,16)	(2,14)
t_{18}	(4,17)	(2,15)
t_{19}	(5,18)	(3,16)
t_{20}	(6,19)	(4,17)
t_{21}	(7,19)	(5,18)
t_{22}		(6,18)

(b)

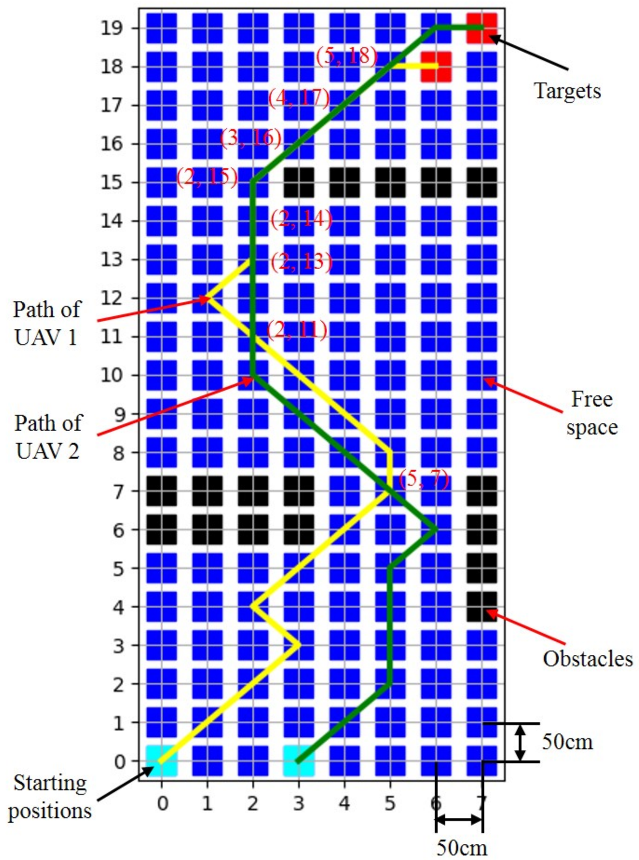

Time steps	UAV 1	UAV 2
t_1	(0, 0)	(3, 0)
t_2	(1, 1)	(4, 1)
t_3	(2, 2)	(5, 2)
t_4	(3, 3)	(5, 3)
t_5	(3, 5)	(5, 4)
t_6	(3, 5)	(5, 5)
t_7	(3, 5)	(6, 6)
t_8	(3, 5)	(5, 7)
t_9	(3, 5)	(4, 8)
t_{10}	(4, 6)	(3,9)
t_{11}	(5, 7)	(2, 10)
t_{12}	(5, 8)	(2, 11)
t_{13}	(5, 8)	(2, 12)
t_{14}	(4, 9)	(2, 13)
t_{15}	(3, 10)	(2, 14)
t_{16}	(2, 11)	(2, 15)
t_{17}	(1, 12)	(3, 16)
t_{18}	(2, 13)	(4, 17)
t_{19}	(2, 14)	(5, 18)
t_{20}	(2, 15)	(6, 19)
t_{21}	(3, 16)	(7, 19)
t_{22}	(4, 17)	
t_{23}	(5, 18)	
t_{24}	(6, 18)	

Fig. 18 Path planning for dual UAVs using (a) original and (b) enhanced SSTM

Field experiment is conducted to illustrate the feasibility of UAVs indoor navigation, **Fig. 19** shows the flight trajectories of two UAVs (highlighted by red and yellow polylines in the 3D model) and the real-time imagery data and video clips collected by the UAVs. The UAVs fly from the starting positions to the corresponding targets in compliance with the optimized Paths (in **Fig. 18**) without colliding with any obstacles. The results indicate that the proposed MARS can simultaneously generate two optimal flight paths for collecting UAV imagery data in cluttered environments.

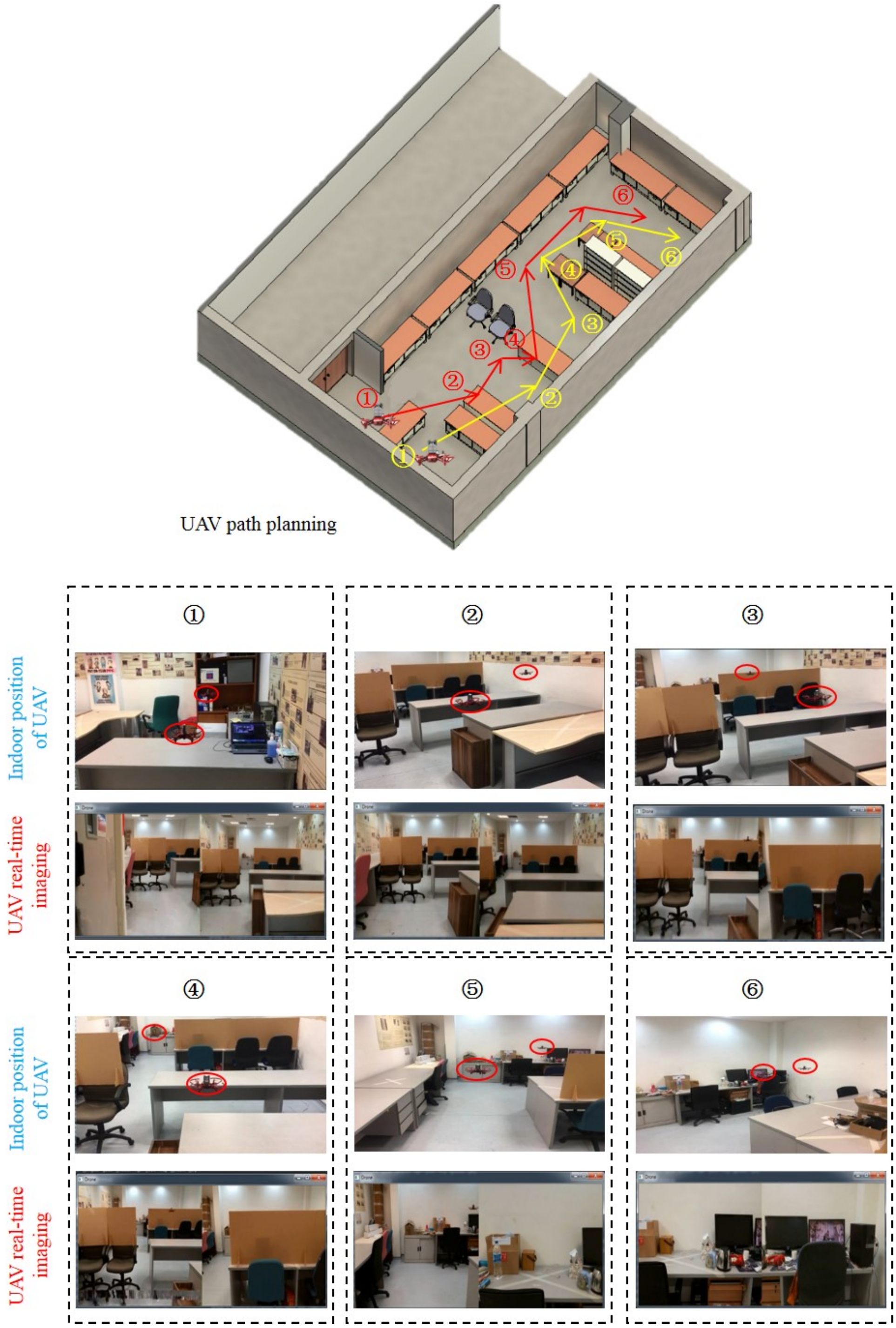

Fig. 19 Indoor navigation and data collection of dual UAVs

4.4 Indoor Navigation for Combined UAV-UGV

The third experiment tests the application of the proposed MARS for controlling UAV and UGV. In this experiment, the UGV is equipped with a 2D LiDAR, a scanning sensor and a platform to carry the UAV. Path planning optimization is performed using enhanced SSTM. The UGV first moves from its starting position on the corridor into the research laboratory. In this process, the UGV takes RGB-D images and generates 3D point clouds using RTABMAP. **Fig. 20** shows the real-time 3D reconstructed scene of the corridor and a portion of the laboratory when UGV moves along its optimized path and collects imagery data. To test multi-robot collaboration, a chair is placed at the laboratory entrance, which prevents the UGV from entering the room (see position 3 in **Fig. 21**). In such a situation, the UGV communicates with the mediating agent and reports an affair requesting the UAV to continue scanning within the laboratory. The mediating agent sends the current grid map (G_E) and target position $P_t = (x_t, y_t)$ to the UAV to conduct path planning optimization, which supports the UAV to automatically flies within the laboratory for collecting image data. **Fig. 21** shows the UAV's flight trajectory (highlighted by a red polyline), and the real-time imagery data and video clips collected by the UAV. The above process is automatic without human intervention. The experimental result shows that the proposed new MARS can potentially support coordination between UAV-UGV toward more automated sensory data collection. Besides, different forms of information such as images and 3D point clouds can be collected using MARS.

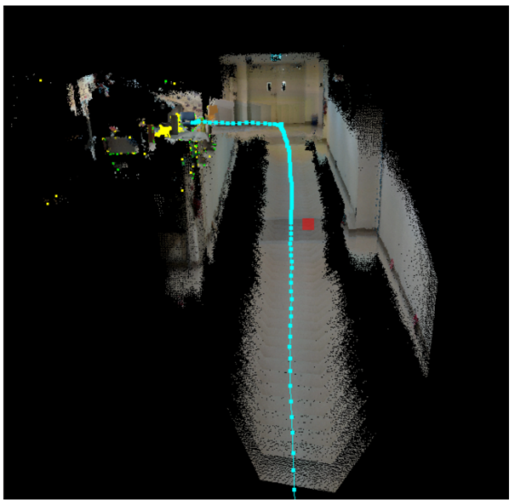

Fig. 20 3D reconstructed scene of the construction research laboratory

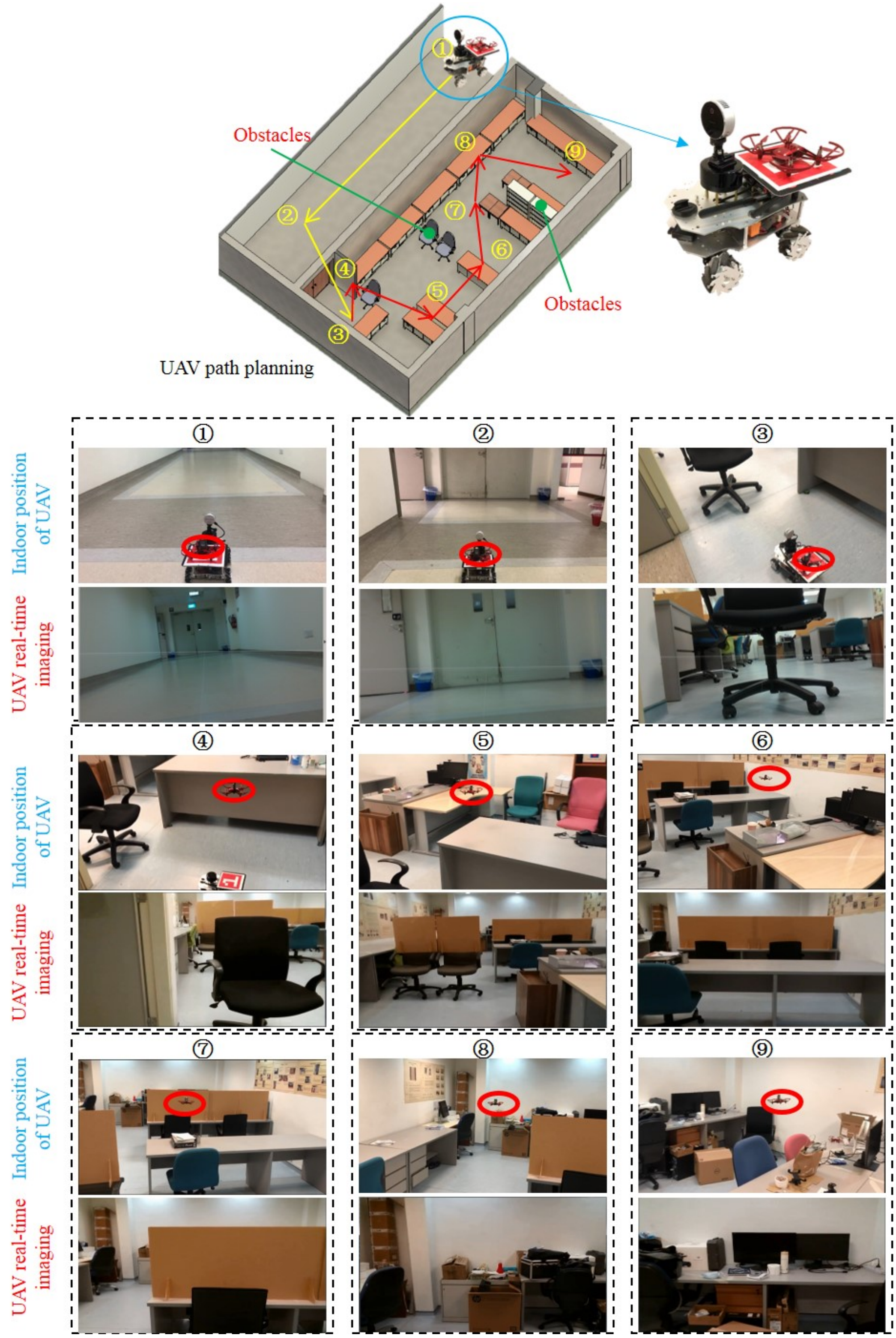

Fig. 21 Indoor navigation and data collection using combined UAV-UGV

5. CONCLUSIONS

This paper presents a new MARS to automate indoor sensory data collection in cluttered environments. The proposed MARS consists of a new system architecture which defines the attributes and data requirements to support UAV-UGV path planning and indoor navigation. The connection between UAV, UGV, sensing devices, and mediating agents is established. An enhanced SSTM model is proposed to optimize UAV-UGV path planning toward more efficient data collection. The feasibility of path planning for UAV and UGV is verified using simulation and LiDAR-based approaches, respectively. A coordinating control algorithm, including an information exchange mechanism, is developed to resolve the potential conflict and promote coordination between UAV and UGV for automated data collection. Finally, three field experiments are conducted to verify and demonstrate the performance of the proposed MARS. The experiment results show that imagery data and 3D point clouds can be collected using the proposed MARS, which is one of the advantages compared to just using UAV/UGV.

This study provides new insights into automated sensory data collection in cluttered environments. Firstly, it is possible to construct a UAV-UGV system for automatic data collection in a cluttered indoor environment. Secondly, multiple types of sensory data can be collected using a UAV-UGV system, which is beneficial for facility management. Thirdly, a UAV-UGV system can process the collected data in real-time using a low computational complex platform, which is helpful for real-time facility inspection. The present study is one of the early attempts to introduce MARS into indoor navigation of UAV/UGV for automated data collection, but it shows the potential for revolutionizing data collection and indoor inspection.

However, this study has certain limitations. The positioning of UAVs relies on the onboard visual positioning system, which is less accurate. In addition, 2D navigation with the assumption of a fixed UAV flying height is considered in indoor navigation. Future work for this study shall include integrating advanced localization techniques, such as visual SLAM, into the MARS for more accurate indoor localization. Furthermore, different kinds of robotic devices equipped with various sensors will be leveraged in the future. Algorithms dealing with 3D cooperative navigation shall be developed to use different robots for indoor inspection.

ACKNOWLEDGEMENTS

This research was funded by NUS Start-up Grant (No. R-296-000-233-133). Any opinions and findings are those of the authors and do not necessarily reflect the views of the grantor.

REFERENCES

[1] Q. Lu, X. Xie, A.K. Parlikad, J.M. Schooling, Digital twin-enabled anomaly detection for built asset monitoring in operation and maintenance, Automation in Construction 118 (2020) 103277, https://doi.org/10.1016/j.autcon.2020.103277.

[2] M.Y.T. Chew, K. Yan, Enhancing Interpretability of Data-Driven Fault Detection and Diagnosis Methodology with Maintainability Rules in Smart Building Management, Journal of Sensors (2022), https://doi.org/10.1155/2022/5975816.

[3] J. Moore, H. Tadinada, K. Kirsche, J. Perry, F. Remen, Z.T.H. Tse, Facility inspection using UAVs: a case study in the University of Georgia campus, International journal of remote sensing 39(21) (2018) 7189-7200, https://doi.org/10.1080/01431161.2018.1515510.

[4] S.H.H. Shah, O.-M.H. Steinnes, E.G. Gustafsson, I.A. Hameed, Multi-Agent Robot System to Monitor and Enforce Physical Distancing Constraints in Large Areas to Combat COVID-19 and Future Pandemics, Applied Sciences 11(16) (2021) 7200, https://doi.org/10.3390/app11167200.

[5] V. Prabakaran, M.R. Elara, T. Pathmakumar, S. Nansai, Floor cleaning robot with reconfigurable mechanism, Automation in Construction 91 (2018) 155-165, https://doi.org/10.1016/j.autcon.2018.03.015.

[6] A.K. Lakshmanan, R.E. Mohan, B. Ramalingam, A.V. Le, P. Veerajagadeshwar, K. Tiwari, M. Ilyas, Complete coverage path planning using reinforcement learning for tetromino based cleaning and maintenance robot, Automation in Construction 112 (2020) 103078, https://doi.org/10.1016/j.autcon.2020.103078.

[7] K. Yan, Z. Xiaokang, Chiller faults detection and diagnosis with sensor network and adaptive 1D CNN, Digital Communications and Networks (2022), https://doi.org/10.1016/j.dcan.2022.03.023.

[8] M. Jin, S. Liu, S. Schiavon, C. Spanos, Automated mobile sensing: Towards high-granularity agile indoor environmental quality monitoring, Building and Environment 127 (2018) 268-276, https://doi.org/10.1016/j.buildenv.2017.11.003.

[9] P. Ribino, M. Bonomolo, C. Lodato, G. Vitale, A humanoid social robot based approach for indoor environment quality monitoring and well-being improvement, International Journal of Social Robotics (2020) 1-20, https://doi.org/10.1007/s12369-020-00638-9.

[10] K. Asadi, A.K. Suresh, A. Ender, S. Gotad, S. Maniyar, S. Anand, M. Noghabaei, K. Han, E. Lobaton, T. Wu, An integrated UGV-UAV system for construction site data collection, Automation in Construction 112 (2020) 103068, https://doi.org/10.1016/j.autcon.2019.103068.

[11] K. Asadi, H. Ramshankar, H. Pullagurla, A. Bhandare, S. Shanbhag, P. Mehta, S. Kundu, K. Han, E. Lobaton, T. Wu, Vision-based integrated mobile robotic system for real-time applications in construction, Automation in construction 96 (2018) 470-482, https://doi.org/10.1016/j.autcon.2018.10.009.

[12] B. Grocholsky, J. Keller, V. Kumar, G. Pappas, Cooperative Air and Ground Surveillance, IEEE Robotics & Automation Magazine 13(3) (2006) 16-25, https://doi.org/10.1109/MRA.2006.1678135.

[13] N. Giakoumidis, J.U. Bak, J.V. Gómez, A. Llenga, N. Mavridis, Pilot-Scale Development of a UAV-UGV Hybrid with Air-Based UGV Path Planning, 2012 10th International Conference on Frontiers of Information Technology, 2013, pp. 204-208.

[14] P. Fankhauser, M. Bloesch, P. Krüsi, R. Diethelm, M. Wermelinger, T. Schneider, M. Dymczyk, M. Hutter, R. Siegwart, Collaborative navigation for flying and walking robots, 2016 IEEE/RSJ International Conference on Intelligent Robots and Systems (IROS), IEEE, 2016, pp. 2859-2866.

[15] N. Michael, S. Shen, M. Kartik, Y. Mulgaonkar, V. Kumar, K. Nagatani, Y. Okada, S. Kiribayashi, K. Otake, K. Yoshida, K. Ohno, E. Takeuchi, S. Tadokoro, Collaborative mapping of an earthquake-damaged building via ground and aerial robots, Journal of Field Robotics 29(5) (2012) 832-841, https://doi.org/10.1002/rob.21436.

[16] N. Michael, S. Shen, K. Mohta, V. Kumar, K. Nagatani, Y. Okada, S. Kiribayashi, K. Otake, K. Yoshida, K. Ohno, Collaborative mapping of an earthquake damaged building via ground and aerial robots, Field and service robotics, Springer, 2014, pp. 33-47.

[17] E. Mueggler, M. Faessler, F. Fontana, D. Scaramuzza, Aerial-guided navigation of a ground robot among movable obstacles, 2014 IEEE International Symposium on Safety, Security, and Rescue Robotics (2014), IEEE, 2014, pp. 1-8.

[18] P. Kim, L.C. Price, J. Park, Y.K. Cho, UAV-UGV Cooperative 3D Environmental Mapping, ASCE International Conference on Computing in Civil Engineering 2019, 2019, pp. 384-392.

[19] S. Kemp, J. Rogers, UAV-UGV Teaming for Rapid Radiological Mapping, 2021 IEEE International Symposium on Safety, Security, and Rescue Robotics (SSRR), 2021, pp. 92-97.

[20] J. Park, P. Kim, Y.K. Cho, Automated collaboration framework of UAV and UGV for 3D visualization of construction sites, Proceedings of the 18th International Conference on Construction Applications of Virtual Reality (CONVR2018), 2018.
[21] P. Rea, E. Ottaviano, Design and development of an Inspection Robotic System for indoor applications, Robotics and Computer-Integrated Manufacturing 49 (2018) 143-151, https://doi.org/10.1016/j.rcim.2017.06.005.
[22] B.R. Mantha, C.C. Menassa, V.R. Kamat, Robotic data collection and simulation for evaluation of building retrofit performance, Automation in Construction 92 (2018) 88-102, https://doi.org/10.1016/j.autcon.2018.03.026.
[23] S. Kim, M. Peavy, P.-C. Huang, K. Kim, Development of BIM-integrated construction robot task planning and simulation system, Automation in Construction 127 (2021) 103720, https://doi.org/10.1016/j.autcon.2021.103720.
[24] N. Bolourian, A. Hammad, LiDAR-equipped UAV path planning considering potential locations of defects for bridge inspection, Automation in construction 117 (2020) 103250, https://doi.org/10.1016/j.autcon.2020.103250.
[25] C. Song, K. Wang, J.C.P. Cheng, BIM-Aided Scanning Path Planning for Autonomous Surveillance UAVs with LiDAR, ISARC. Proceedings of the International Symposium on Automation and Robotics in Construction 2020 2020, pp. 1195-1202.
[26] Y. Khosiawan, I. Nielsen, A system of UAV application in indoor environment, Production & Manufacturing Research 4(1) (2016) 2-22, https://doi.org/10.1080/21693277.2016.1195304.
[27] J.A. Guerrero, Y. Bestaoui, UAV Path Planning for Structure Inspection in Windy Environments, Journal of Intelligent & Robotic Systems 69 (2013) 297–311, https://doi.org/10.1007/s10846-012-9778-2.
[28] d.S.L. González, N.E. Frías, S.J. Martínez, J.H. González, Indoor path-planning algorithm for UAV-based contact inspection, Sensors 21(2) (2021) 642, https://doi.org/10.3390/s21020642.
[29] H. Freimuth, M. Sonig, Planning and executing construction inspections with unmanned aerial vehicles, Automation in construction 96 (2018), https://doi.org/10.1016/j.autcon.2018.10.016.
[30] A. Lakas, B. Belkhouche, O. Benkraouda, A. Shuaib, H.J. Alasmawi, A framework for a cooperative UAV-UGV system for path discovery and planning, 2018 International Conference on Innovations in Information Technology (IIT), IEEE, 2018, pp. 42-46.
[31] P. Kim, J. Park, Y. Cho, As-is Geometric Data Collection and 3D Visualization through the Collaboration between UAV and UGV, ISARC. Proceedings of the International Symposium on Automation and Robotics in Construction, IAARC Publications, 2019, pp. 544-551.
[32] G. Christie, A. Shoemaker, K. Kochersberger, P. Tokekar, L. McLean, A. Leonessa, Radiation search operations using scene understanding with autonomous UAV and UGV, Journal of Field Robotics 34(8) (2017) 1450-1468, https://doi.org/10.1002/rob.21723.
[33] P. Kim, J. Park, Y.K. Cho, J. Kang, UAV-assisted autonomous mobile robot navigation for as-is 3D data collection and registration in cluttered environments, Automation in Construction 106 (2019) 102918, https://doi.org/10.1016/j.autcon.2019.102918.
[34] A. Cantieri, M. Ferraz, G. Szekir, M.A. Teixeira, J. Lima, A.S. Oliveira, M.A. Wehrmeister, Cooperative UAV–UGV autonomous power pylon inspection: An investigation of cooperative outdoor vehicle positioning architecture, Sensors 20(21) (2020) 6384, https://doi.org/10.3390/s20216384.
[35] F. Guinand, H. Pelvillain, F. Guérin, J.-F. Brethé, A decentralized interactive architecture for aerial and ground mobile robots cooperation, 2015 International Conference on Control, Automation and Robotics, IEEE, 2015, pp. 37-43.
[36] H. Qin, Z. Meng, W. Meng, X. Chen, H. Sun, F. Lin, M.H. Ang, Autonomous exploration and mapping system using heterogeneous UAVs and UGVs in GPS-denied environments, IEEE Transactions on Vehicular Technology 68(2) (2019) 1339-1350, https://doi.org/10.1109/TVT.2018.2890416.
[37] Á. Madridano, A. Al-Kaff, D. Martín, Trajectory planning for multi-robot systems: Methods and applications, Expert Systems with Applications (2021) 114660, https://doi.org/10.1016/j.eswa.2021.114660.
[38] A.L. Hodgkin, A.F. Huxley, A quantitative description of membrane current and its application to conduction and excitation in nerve, The Journal of physiology 117(4) (1952) 500-544, https://doi.org/10.1113/jphysiol.1952.sp004764.
[39] S. Grossberg, Nonlinear neural networks: Principles, mechanisms, and architectures, Neural networks 1(1) (1988) 17-61, https://doi.org/10.1016/0893-6080(88)90021-4.
[40] R. Glasius, A. Komoda, S.C. Gielen, Neural network dynamics for path planning and obstacle

avoidance, Neural Networks 8(1) (1995) 125-133, https://doi.org/10.1016/0893-6080(94)E0045-M.
[41] S.X. Yang, M. Meng, An efficient neural network method for real-time motion planning with safety consideration, Robotics and Autonomous Systems 32(2-3) (2000) 115-128, https://doi.org/10.1016/S0921-8890(99)00113-X.
[42] H. Liu, J. Ma, W. Huang, Sensor-based complete coverage path planning in dynamic environment for cleaning robot, CAAI Transactions on Intelligence Technology 3(1) (2018) 65-72, https://doi.org/10.1049/trit.2018.0009.
[43] S.X. Yang, M. Meng, Neural network approaches to dynamic collision-free trajectory generation, IEEE Transactions on Systems, Man, and Cybernetics, Part B (Cybernetics) 31(3) (2001) 302-318, https://doi.org/10.1109/3477.931512.
[44] H. Li, S.X. Yang, M.L. Seto, Neural-network-based path planning for a multirobot system with moving obstacles, IEEE Transactions on Systems, Man, and Cybernetics, Part C (Applications and Reviews) 39(4) (2009) 410-419, https://doi.org/10.1109/TSMCC.2009.2020789.
[45] M. Meng, X. Yang, A neural network approach to real-time trajectory generation [mobile robots], Proceedings. 1998 IEEE International Conference on Robotics and Automation (Cat. No. 98CH36146), IEEE, 1998, pp. 1725-1730.
[46] S.X. Yang, M. Meng, An efficient neural network approach to dynamic robot motion planning, Neural networks 13(2) (2000) 143-148, https://doi.org/10.1016/S0893-6080(99)00103-3.